IEEE Access
Multidisciplinary | Rapid Review | Open Access Journal

SPECIAL SECTION ON ADVANCES IN MACHINE LEARNING AND COGNITIVE COMPUTING FOR INDUSTRY APPLICATIONS

Received June 27, 2020, accepted July 23, 2020, date of publication July 27, 2020, date of current version August 7, 2020.

Digital Object Identifier 10.1109/ACCESS.2020.3012196

Deep Learning Aided Dynamic Parameter Identification of 6-DOF Robot Manipulators

SHOUJUN WANG[1,2], XINGMAO SHAO[1,2], LIUSONG YANG[3], AND NAN LIU[1,2]

[1]National Demonstration Center for Experimental Mechanical and Electrical Engineering Education, Tianjin University of Technology, Tianjin 300384, China
[2]Tianjin Key Laboratory for Advanced Mechatronic System Design and Intelligent Control, Tianjin University of Technology, Tianjin 300384, China
[3]CITIC Heavy Industries Company Ltd., Luoyang 471003, China

Corresponding author: Nan Liu (tjutnan@hotmail.com)

This work was supported by the National Key Research and Development Program of China under Grant 2017YFB1302100.

ABSTRACT Generally, structural uncertainty of the robot dynamics system refers to model error caused by parameter identification, unstructured uncertainty is the unmodeled dynamic characteristic. No matter how elaborate modeling methods are used, there always be uncertainty. Therefore, this article applies deep learning for the first time to aid robot dynamic parameter identification of 6 degrees of freedom robot manipulator for compensation of uncertain factors. Firstly, the relatively accurate prediction of torque is obtained by the physical dynamic model using the parameters identification method (errors are less than 10% of the maximum torques). Secondly, we propose a novel deep neural network based approach called Uncertainty Compensation Model (UCM) to compensate the torque error introduced by the uncertainty. The UCM mainly composed by proposed Input Control Module (ICM) and Error Learning Models (ELMs) based on Long-Short-Term Memory and attention mechanism. The proposed ICM, which effectively avoids the unnecessary interference, is used to control valid input for ELMs. The ELMs, consisted by ELM units, concern extracting salient features from sequence data to predict the joint error. Also, this article summarizes the effects of valid input, timestep and attention mechanism on the performance of the UCM. Finally, the verification of parameter identification and torques compensation is carried out by a Universal Robot 5 manipulator. Compared with the prediction torques of physical dynamic model, the proposed UCM has a good ability to capture the friction characteristics and compensate for the error of local maximum torques, which effectively solves the deficiency of the physical dynamics model and improves prediction accuracy (errors are less than 6% of the maximum torques).

INDEX TERMS Deep learning, inverse dynamics, LSTM, parameter identification, robot, torques compensation.

I. INTRODUCTION

The precise torque prediction of robot is a prerequisite for precise control of the industrial robot. High-speed and high-precision motion schemes place higher requirements on control methods. Meanwhile, accurate identification of the robot's dynamic parameters is the key to establishing a rigid-body dynamic model of the robot and the basis for achieving high-precision control. Generally, the uncertain factors of robot dynamics system are divided into structural and non-structural uncertainties. The errors of identification parameter introduce structural uncertainty. Many factors, such as joint nonlinear damping, friction model design methods, and noise, are non-structural uncertainty, and to express uncertain factors through physical modeling methods is challenging. Therefore, for general industrial robots, it is important to develop a reasonable and applicable torque prediction methods.

Many manufacturers do not provide or partially provide robot dynamics parameters [1], [2], also, since factor of manufacturing errors, uneven material distribution and so on, the dynamic parameters of industrial robots of the same model may differ. However, due to the complexity of most robots, it is impractical to measure physical parameters directly [3]. Experiments are still the most effective way to obtain dynamic parameters. Gautier [4] proposed a dynamic parameter identification method based on the energy equation and obtained an identification model without joint angular acceleration, which avoids the introduction of high-frequency noise. The Newton-Euler method,

The associate editor coordinating the review of this manuscript and approving it for publication was Min Xia.

This work is licensed under a Creative Commons Attribution 4.0 License. For more information, see https://creativecommons.org/licenses/by/4.0/

which establishes a dynamic equation from the perspective of force equilibrium, is widely cited [5], and its iterative properties are conducive to computer implementation. The dynamic characteristics of the robot are linearly related to its dynamic parameters laying a theoretical foundation for the dynamic parameter identification of serial robots.

Generally, non-structural uncertainty is the main factor that causes inaccurate identification parameters. Zhang *et al.* considered the joint stiffness into the dynamic model and improved the accuracy of identification [6]. The noise disturbs joint angles and currents, and the optimization of the excitation trajectory can reduce the impact of measurement noise on identification accuracy. Atkeson *et al.* proposed a fifth-order polynomial trajectory as the excitation trajectory in [7]. The trajectory design method based on the Fourier series can improve the signal-noise ratio [8], [9]. The common method for constructing a finite Fourier series trajectory is based on the minimum condition number of the coefficient matrix of the linearized dynamic equation [10].

For parameter estimation methods, the least squares method [11], weighted least squares method [12], and maximum likelihood estimation method [9] are popular approaches. Machine learning has the nonlinear fitting ability, which is used to solve the problem of robot parameter identification. Wang *et al.* established a shallow neural network to identify the dynamic parameters of the reconfigurable robot [13]. In terms of identification strategy, The one-step identification method easily overwhelms joint parameters with small torque coefficients due to joint coupling. The step-by-step identification method can optimize the identification process and effectively improve identification accuracy [12].

Machine learning is a typical research hotspot in the field of artificial intelligence and pattern recognition. Polydoros *et al.* proposed a machine learning algorithm for online modeling of robot inverse dynamics and implemented the algorithm for torque calculation on real robots [14]. The artificial neural network model is one of machine learning, it learns statistical laws from a large number of training samples to predict unknown laws. Duc *et al.* used a neural network to design a neural network controller that conforms to the robot dynamic characteristics [15]. Deep learning exploits the property that many natural signals are compositional hierarchies, where higher-level features are obtained by composing lower-level ones. Compared with shallow neural networks, deep learning has better feature learning capabilities and an essential characterization of the data. The training of deep learning requires a large amount of data, and the accuracy of the identification depends mostly on the quality of the data [16]. Recently, some deep learning methods, such as deep neural networks and recurrent neural networks, have been applied in the field of robotics. Binyan *et al.* proposed the use of deep neural networks to calculate robot dynamics and performed physical simulations [17].

The recurrent neural network is a kind of deep learning especially suitable for learning time series data. Time series prediction can be summarized as the process of extracting useful information from historical records and determining future values [18]. The Long-Short-Term Memory (LSTM) model uses LSTM cells as hidden layers to avoid gradient disappearance and gradient explosion and solves the problem that the recurrent neural network cannot handle long-distance dependencies [19], [20]. Liu *et al.* established the mapping between robot joint motion and torque through LSTM technology to predict the torque based on robot joint motion and achieved good results [21]. Chaki *et al.* used simple recurrent neural networks and LSTM to learn robot dynamics models and compared them with other regression algorithms, demonstrating the superiority of LSTM models [22].

Although the deep learning method for torque prediction effectively improves the torque tracking accuracy, the deep learning network structure and parameters cannot reflect the actual physical meaning of the robot system. Meanwhile, the method of directly establishing a model using neural networks to achieve high-precision dynamic torque calculations has not been well solved in the entire reachable state space of the robot. In robot workspaces that not be trained in deep learning, torque prediction using only deep learning may cause large deviations, leading to fallacious torque prediction. Moreover, the dynamics with identification parameters only cannot consider uncertain factors and it is difficult to predict the torque extremely accurately. However, the physical dynamics model can avoid the shortcoming of the wrong predicted torque produced by the neural network in the untrained workspace.

Focusing on the problem discussed above, the main goal of this work is to develop a robust method combining dynamic parameter identification and deep learning model for compensation of uncertainty. Firstly, parameter identification concerns building a relatively accurate physical dynamics model, which means the torque error of each joint is less than 10% of the maximum torque and guarantees no large torque deviation during torque prediction. Secondly, the strong nonlinear fitting ability of deep learning provides the possibility to consider the uncertainty, which used to establish the mapping between robot motions and the torque error, thus the compensated prediction torque approximate the real value more precise, which mean the compensated torque errors are less than 6% of the maximum torques. More specifically, the main contributions of this work are summarized as follows:

- We carried out a dynamic parameter identification experiment on the UR5 manipulator and published the reference values of its dynamic parameters.
- We proposed a novel deep neural architecture called Uncertainty Compensation Model (UCM) to compensate the torque error introduced by the uncertainty, which has a good ability to capture the friction characteristics and compensate the error of local maximum torques and effectively solves the deficiency of the dynamic model based solely on identification parameters.

- We analyzed the relationship between joints motion and errors compensation, that is, the effect of valid input data on the compensation model, and proposed an input control method, called the Input Control Module (ICM).
- We summarized the effects of valid input, timestep and attention mechanism on the performance of the proposed UCM.

The rest of this article is organized as follows. Section 2 introduces the methods of robot dynamic parameter identification. Section 3 describes the proposed uncertainty compensation architecture based on deep learning. Section 4 illustrates the experimental results of dynamic parameter identification and evaluation of the proposed compensation model and examines the proposed method by a verification trajectory. Finally, Section 5 summarizes the conclusions.

II. DYNAMIC MODEL AND IDENTIFICATION

A. DYNAMICS IDENTIFICATION MODEL

The primary purpose of robot dynamics is to achieve real-time control, and accurate dynamic models and precise dynamic parameters are the keys. The dynamics of robot can be expressed by the Lagrange method or the Newton-Euler method. The Newton-Euler method has high calculation efficiency, and its expression is as follows:

$$\boldsymbol{\tau} = \boldsymbol{M}(\boldsymbol{q})\ddot{\boldsymbol{q}} + \boldsymbol{H}(\boldsymbol{q}, \dot{\boldsymbol{q}}) + \boldsymbol{G}(\boldsymbol{q}) + \boldsymbol{\xi} \tag{1}$$

where $\boldsymbol{q}, \dot{\boldsymbol{q}}, \ddot{\boldsymbol{q}}$ are the vectors of joint position, velocity, and acceleration, respectively, n represents the degrees of freedom (DOF) of a robot. $\boldsymbol{\tau}$ is the vector of joint torques, $\boldsymbol{M}(\boldsymbol{q}) \in R^{n\times n}$ is the inertia matrix, $\boldsymbol{H}(\boldsymbol{q}, \dot{\boldsymbol{q}}) \in R^n$ is the vector of centrifugal and Coriolis forces, $\boldsymbol{G}(\boldsymbol{q}) \in R^n$ is the vector of gravitational torque or force, $\boldsymbol{\xi} \in R^n$ is the offset torques which denotes uncertain influence factors of dynamic.

Non-linear friction factors are the main factors affecting the robot's high-precision motion. The Coulomb viscous friction model is adopted to the robot dynamics identification model to represent the effect of friction on robot dynamics:

$$\boldsymbol{\xi} = f_v\dot{\boldsymbol{q}} + f_c sign(\dot{\boldsymbol{q}}) + \boldsymbol{\epsilon}(\boldsymbol{q}, \dot{\boldsymbol{q}}, \ddot{\boldsymbol{q}}) \tag{2}$$

where f_v, f_c are viscosity and Coulomb friction coefficient, respectively, $\boldsymbol{\epsilon}(\boldsymbol{q}, \dot{\boldsymbol{q}}, \ddot{\boldsymbol{q}}) \in R^n$ represents factors unmodeled in physical dynamic model.

The inertia parameters affect the robot's motion performance significantly when the robot is running at high speed [12], the inertia parameter vector $\boldsymbol{\pi_i}$ of link i can be expressed as:

$$\boldsymbol{\pi_i} = (XX_i, XY_i, XZ_i, YY_i, YZ_i, ZZ_i, MX_i, MY_i, MZ_i, M_i, f_{vi}, f_{ci})^T$$

where $(XX_i, XY_i, XZ_i, YY_i, YZ_i, ZZ_i)^T$ is the inertia tensor of the link i relative to the origin of the coordinate system i, MX_i, MY_i, MZ_i is the first-order moment of inertia of the link i, and M_i is the mass of the link i.

Khalil proposed a method to determine the minimum inertial parameter set of a tree-structured robot in [23]. Since the link dynamic parameters are redundant to determine the manipulator dynamic model uniquely, the observation matrix of inverse dynamic identification model is not often a full-rank matrix. The minimum inertia parameters set can be obtained by reducing and eliminating the linear correlation terms in the observation matrix [12]. The inverse dynamic identification model is [24]:

$$\boldsymbol{\tau} = \boldsymbol{\Phi}(\boldsymbol{q}, \dot{\boldsymbol{q}}, \ddot{\boldsymbol{q}})\boldsymbol{\beta} + \boldsymbol{\epsilon}(\boldsymbol{q}, \dot{\boldsymbol{q}}, \ddot{\boldsymbol{q}}) \tag{3}$$

where $\boldsymbol{\Phi}(\boldsymbol{q}, \dot{\boldsymbol{q}}, \ddot{\boldsymbol{q}}) \in R^{n\times m}$ is the observation matrix, m, n are the number of parameters in the minimum inertia parameter set and the totality of link, respectively, and $\boldsymbol{\beta} \in R^{m\times 1}$ is the minimum inertia parameter set.

It is necessary to utilize the excitation trajectory to excite the robot system continuously. After sampling and processing the robot position, velocity, and acceleration data $(\hat{\boldsymbol{q}}, \hat{\dot{\boldsymbol{q}}}, \hat{\ddot{\boldsymbol{q}}})$ at a specific frequency, these measured data is used to obtain the linear over-determined equation:

$$\boldsymbol{\tau_M} = \boldsymbol{\Phi_M}(\hat{\boldsymbol{q}}, \hat{\dot{\boldsymbol{q}}}, \hat{\ddot{\boldsymbol{q}}})\boldsymbol{\beta} + \boldsymbol{\epsilon}(\hat{\boldsymbol{q}}, \hat{\dot{\boldsymbol{q}}}, \hat{\ddot{\boldsymbol{q}}}) \tag{4}$$

where

$$\boldsymbol{\Phi_M} = \begin{bmatrix} \Phi\left(q\left(t_1\right), \dot{q}\left(t_1\right), \ddot{q}\left(t_1\right)\right)_{n\times m} \\ \Phi\left(q\left(t_2\right), \dot{q}\left(t_2\right), \ddot{q}\left(t_2\right)\right)_{n\times m} \\ \vdots \\ \Phi\left(q\left(t_N\right), \dot{q}\left(t_N\right), \ddot{q}\left(t_N\right)\right)_{n\times m} \end{bmatrix} \in R^{Nn\times m} \tag{5}$$

is the observation matrix and $\boldsymbol{\tau_M} \in R^{Nn\times 1}$ is the measured torque, $\boldsymbol{\epsilon}(\hat{\boldsymbol{q}}, \hat{\dot{\boldsymbol{q}}}, \hat{\ddot{\boldsymbol{q}}}) \in R^{Nn\times 1}$ is the measured error, N is the number of sampling points over one period of periodic trajectory.

B. PARAMETER IDENTIFICATION METHOD OF LEAST SQUARES

We use the least squares identification method to solve over-determined equations [5]:

$$\hat{\boldsymbol{\beta}} = min\left\|\boldsymbol{\tau_M} - \boldsymbol{\Phi_M}\hat{\boldsymbol{\beta}}\right\| = \left(\boldsymbol{\Phi_M^T}\boldsymbol{\Phi_M}\right)^{-1}\boldsymbol{\Phi_M^T}\boldsymbol{\tau_M} \tag{6}$$

where $\hat{\boldsymbol{\beta}}$ is the predicted base parameter vector, which represents the identifiable parameters of robot dynamics. The solution $\hat{\boldsymbol{\beta}}$ is validated with the classical base parameter estimation method [25]. σ_ϵ^2 is the unbiased estimation of standard deviation of $\boldsymbol{\epsilon}$:

$$\sigma_\epsilon^2 = \frac{1}{Nn-m}\left\|\boldsymbol{\tau_M} - \boldsymbol{\Phi_M}\hat{\boldsymbol{\beta}}\right\|^2 \tag{7}$$

The covariance matrix of the estimated parameters can be written as:

$$C_{\hat{\boldsymbol{\beta}}} = E\left[\left(\boldsymbol{\beta} - \hat{\boldsymbol{\beta}}\right)\left(\boldsymbol{\beta} - \hat{\boldsymbol{\beta}}\right)^T\right] = \sigma_\epsilon^2(\boldsymbol{\Phi_M^T}\boldsymbol{\Phi_M})^{-1} \tag{8}$$

The standard deviation of the j^{th} parameter is included in the diagonal element of $C_{\hat{\beta}}$:

$$\sigma_{\hat{\beta}_j} = \sqrt{C_{\hat{\beta}}(j,j)} \tag{9}$$

The relative standard deviation can be expressed as:

$$\sigma_{\hat{\beta}_{jr}}\% = 100\frac{\sigma_{\hat{\beta}_j}}{\left|\hat{\beta}_j\right|} \tag{10}$$

C. EXCITATION TRAJECTORY AND SIGNAL PROCESSING

An ideal excitation trajectory can fully excite the dynamic parameters to improve the identification accuracy. The excitation trajectory of the finite Fourier series is extensively used [9]:

$$q_i(t) = q_{i,0} + \sum_{k=1}^{z}\left(a_{i,k}\sin\left(kw_f t\right) + b_{i,k}\cos\left(kw_f t\right)\right) \tag{11}$$

where w_f is the fundamental frequency and $q_{i,0}$ is the offset of the joint position of excitation trajectories of each joint $q_i(t)$. The parameters $a_{i,k}$ and $b_{i,k}$ $(k = 1, 2, \ldots, z)$ are the amplitudes of the cosine and sine functions and can be optimized through minimizing condition number of the regression matrix $\boldsymbol{\Phi_M}$.

General industrial robots do not equip torque sensors. The measured torque is generally obtained indirectly through the motor current. The relationship between torque and current is:

$$\tau_i = K_i R_i i_i \tag{12}$$

where K_i is the motor torque constant, R_i is the transmission ratio between the motor and the link, i_i is the motor current.

Generally, the signals acquired from the robot controller are the position and speed measurements while the robot is tracking the planned excitation trajectory. Averaging the data can increase the signal-to-noise ratio of the data [12], the average position $\bar{q}$ can be expressed by:

$$\bar{q}(k) = \frac{1}{S}\sum_{s=1}^{S} q_s(k) \tag{13}$$

where S is the totality of cycles of the trajectory, $q_s(k)$ is the k^{th} sampling point of an exciting trajectory, $\bar{q}(k)$ is the position after averaging. The processing of improving the signal-noise ratio of speed and current is the same as the processing of position data.

We used a zero-phase lowpass Butterworth filter to process the averaged position and velocity $(\bar{q}, \dot{\bar{q}})$, and the acceleration is obtained by the central difference method. The current measurement is filtered by the Robust LOcal polynomial regrESSion (RLOESS) smoother. RLOESS is a regression method that uses a moving average filter and performs residual analysis to remove outliers before smoothing.

III. DEEP LEARNING BASED COMPENSATION METHOD

A. LONG SHORT-TERM MEMORY

Time series refers to a series of observations recorded in chronological order. It is random data formed by one or more variables at different times, reflecting the development and change of the phenomenon. LSTM cells control the transmission of historical information through gate functions, which has certain time series processing and prediction capabilities.

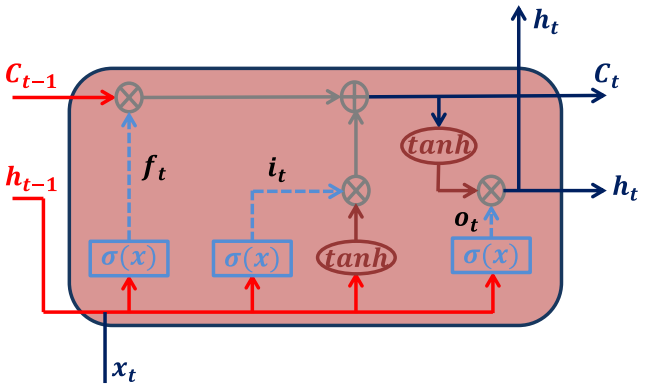

FIGURE 1. The architecture of the LSTM cell.

The LSTM unit is a particular network structure with three "gate" structures, including "forget gate," "input gate," and "output gate." LSTM cells selectively transmit information through the "gate" structure to achieve the purpose of controlling information. Figure 1 shows the schematic diagram, and the following formula expresses the rule of LSTM:

$$f_t = \sigma(W_f \cdot x_t + U_f \cdot h_{t-1} + b_f) \tag{14}$$
$$i_t = \sigma(W_i \cdot x_t + U_i \cdot h_{t-1} + b_i) \tag{15}$$
$$o_t = \sigma(W_o \cdot x_t + U_o \cdot h_{t-1} + b_o) \tag{16}$$
$$C_t = f_t \odot C_{t-1} + i_t \odot \sigma(W_c x_t + U_c h_{t-1} + b_c) \tag{17}$$
$$h_t = o_t \odot tanh(c_t) \tag{18}$$

where f_t, i_t, o_t is the output of the forget gate, input gate, and output gate at the time x_t, respectively; W_f, W_i, W_o, W_c is weight matrix; U_f, U_i, U_o, U_c is the weight matrix of h_{t-1}; b_f, b_i, b_o, b_c is a bias vector, h is the output of the cell unit, C is used to preserve long-term cell state, called the unit state. $\odot$ is the dot product of two vectors. $\sigma(x)$ and $\tanh(x)$ are the sigmoid activation function and the hyperbolic tangent activation function, respectively:

$$\sigma(x) = \frac{1}{1+e^x} \tag{19}$$
$$\tanh(x) = \frac{e^x - e^{-x}}{e^x + e^{-x}} \tag{20}$$

The time sequence of robot inverse dynamics shows that it is more appropriate for learning with LSTM than shallow network structures to model the correlation of time series data to predict the joint torque performance [21]. Meanwhile, theoretically, the longer the timestep size of LSTM, the more information is mined. However, when the timestep exceeds a certain length, long-range memory loss and gradient disappearance still occur. This article solves the gradient dispersion problem by selecting the optimal timestep to extract subsequence features more effectively and retain longer effective memory information.

B. ATTENTION MECHANISMS

The Encoder-Decoder model is popular, which usually encodes the input sequence into a fixed-length vector rep-

resentation. For short-length input sequences, the model can learn a reasonable vector representation, but when the input sequence is very long, learning a reasonable vector representation is difficult. The realization of the attention mechanism is to retain the intermediate output results of the LSTM encoder on the input sequence, and then train a model to selectively learn these inputs, and associate the output sequence with the results of the selective learning when the model is output. The number of operations required to relate signals from two arbitrary input or output positions grows in the distance between positions, This makes it more difficult to learn dependencies between distant positions. Attention mechanisms allow modeling of dependency without regard to their distance in the input or output sequences [26].

A traditional LSTM is applied as the decoder. The hidden states of the decoder denote s, the hidden state s_t generated by the t^{th} decoder cell is computed by:

$$s_t = \mathrm{LSTM}(w_t, s_{t-1}, V_t) \tag{21}$$

where w_t is the input vector, s_{t-1} is the hidden state generated by the last decoder cell. V_t is a weighted sum of hidden states $\{h_1, h_2, \ldots, h_N\}$:

$$V_t = \sum_{u=1}^{N} \alpha_u h_u \tag{22}$$

where α_u is the weight of the hidden layer state of historical input to the current input, which is expressed by:

$$\alpha_u = \frac{\exp(e_u)}{\sum_{i=1}^{N} \exp(e_i)} \tag{23}$$

where the attention function e_u is computed as:

$$e_u = w_a^T \tanh(W_s s_{t-1} + W_h h_u + b_a) \tag{24}$$

where w_a, W_s, W_h and b_a are the parameters to be learned in the attention layer.

The selection of the input sequence is the focus of attention when using the LSTM method for prediction. Without considering the degree of influence of the input sequence on the prediction result, this inevitably reduces the accuracy of the prediction. The Attention mechanism is introduced based on the LSTM model to focus on data sequences that have a key impact on the prediction results. Applying the attention mechanism to the proposed UCM effectively highlight the data that has a key impact on the prediction accuracy, thereby improving the prediction accuracy.

C. PROPOSED INPUT CONTROL MODULE

By deriving the robot dynamics expression, we found that due to the coupling of the dynamics of the tandem manipulator, the identification model of joint i includes not only the dynamic parameters $\boldsymbol{\pi_i}$ of joint i, but also the dynamic parameters $\boldsymbol{\pi_{i+1}}, \ldots, \boldsymbol{\pi_n}$ of joints $i+1, \ldots, n$. Therefore, typical characteristics of tandem robot dynamics are (1) the dynamic parameters of the joint i away from the pedestal influence the torque of joint $1, \ldots, i-1$, but do not affect the motion of its front joint; (2) the joint i near the pedestal has an effect on the motion of joint $i+1, \ldots, n$, but its dynamic parameters have no effect on the torque of the joint behind it. From the above conclusion, we infer that in terms of joint uncertainty compensation, the motion characteristics (position, speed and acceleration) of the joint $i+1, \ldots, n$ are strongly related to the uncertainty compensation of the joint i, however, the motion characteristics of joint i are weakly related or irrelevant to the uncertainty compensation of the joint motion of joint $i+1, \ldots, n$.

Focusing on the above analysis, we have devised a novel Input Control Module (ICM), which is located before the proposed Error Learning Model (ELM) to control the valid input to participate in model training, that is, the motion characteristics of joint $i, i+1, \ldots, n$ join in model learning, when the training target is joint i. Figure 2 shows the proposed uncertainty compensation architecture, which contains the principle of ICM. More specifically, when predicting the torque error of the joint 6, the input motion characteristics are the position, velocity, and acceleration of the joint 6. When predicting the torque error of the joint 5, the input motion characteristics are the position, velocity, and acceleration of joints 5 and 6, and so on. The selection of effective input data by ICM avoids the unnecessary interference of the model, and improves the ability of model's uncertainty compensation.

In the following section, we compared the prediction effect of the torque error when predicting the joint i by inputting the motion information of (1) only the joint i, (2) full input (18 in total for 6-DOF manipulator) and (3) the proposed ICM method, to verify the effectiveness of the proposed method.

D. PROPOSED UNCERTAINTY COMPENSATION MODEL

Based on the problem caused by the uncertain factors of robot dynamics system, this article aims at proposing an uncertainty compensation architecture to predict the torque error caused by uncertainty, which is the torque tracking deviation reflected in high-quality control. The proposed UCM is composed by four components: motion characteristic input layer, ICM layer, ELMs layer and output layer. The specific description of ICM is in Section III.C. The ELMs, consisted by the ELM unit, are the error-learning models based on LSTM and attention mechanism, which concern building an effective mapping of the motion features (output of ICM) and joint torque deviation. The input of ELM unit is determined by ICM, and it has only one output, which is the predicted error value of the target joint. The outputs of the six ELMs correspond to the predicted error values of the six joints of the manipulator. Figure 2 shows the proposed uncertainty compensation architecture and Figure 3 depicts the detailed network architecture of the ELM unit model. The ELM unit model is divided into three layers: encoder layer, re-encoder with attention mechanism layer, and output layer. Specifically, we import the data from ICM into the LSTM to extract the characteristics of the interactive relationship between each timestep, and the output of all timesteps constitutes a new sequence representation related to the original data. Compared with the original data, the new

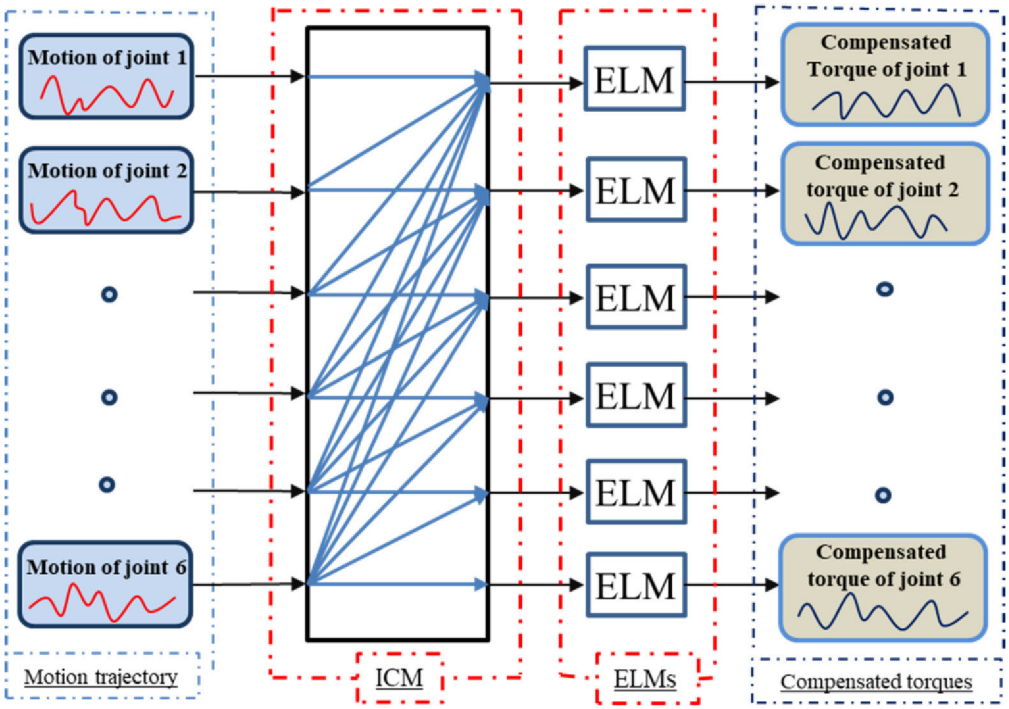

FIGURE 2. The proposed uncertainty compensation architecture.

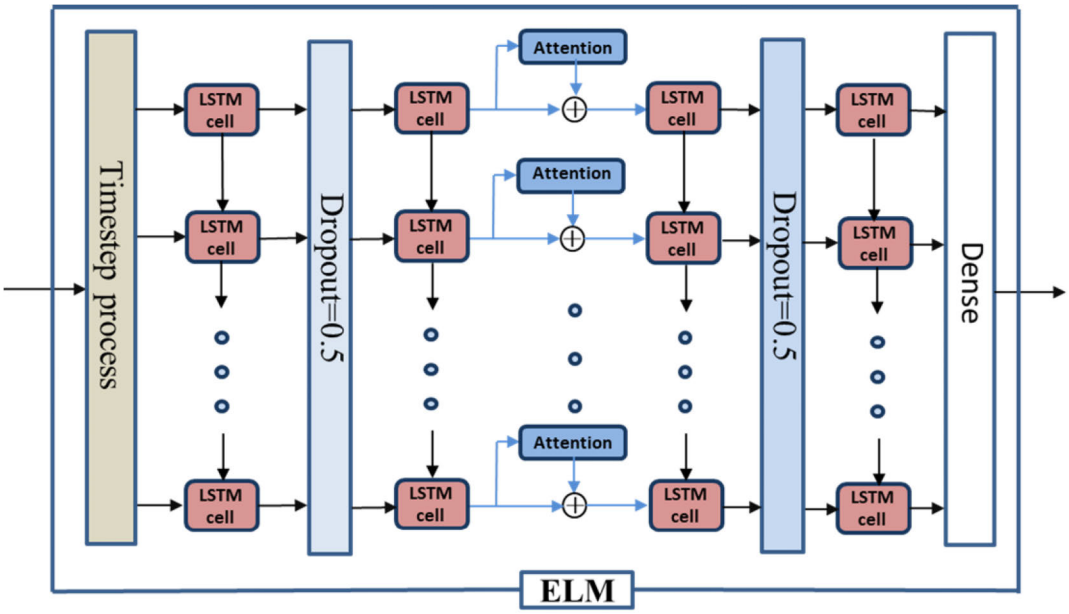

FIGURE 3. The detailed network architecture of the ELM unit model.

representation contains richer time-related data features. The next step is the processing of the re-encoder layer based on the attention mechanism. The output obtained from the encoder layer is used to obtain a new sequence representation with attention weight through an inner product function operation. The attention mechanism makes the model pay attention to the input that has a greater impact on the result prediction. After obtaining a new sequence representation with attention weight, it is merged with the input from the encoder layer and input into the LSTM to further extract attention-based data features. Finally, the outcome of the re-encoder layer is the output layer, which is a fully connected layer, and the final prediction result is obtained.

The experimentally measured data, which are the joint motion characteristics (position, speed and acceleration of six joint) and torque errors (measured torque minus predicted torque calculated by dynamic physical model) at a given timestep, is divided into a training set and a test set. The

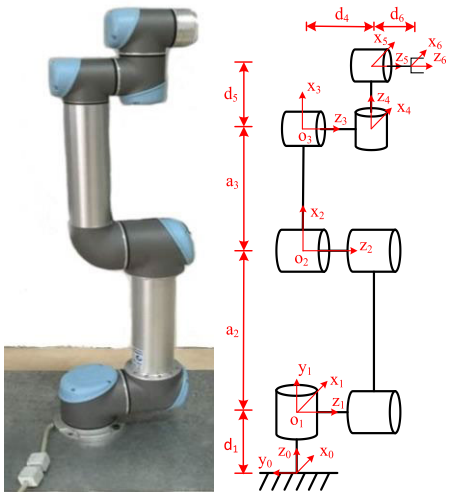

FIGURE 4. The UR5 robot and its link coordinate system.

TABLE 1. The D-H parameters of UR5.

i	α_i	a_i	d_i	θ_i
1	$\pi/2$	0	d_1 (0.08916 m)	θ_1
2	0	a_2 (0.425 m)	0	$\theta_2 - \pi/2$
3	0	a_3 (0.39225 m)	0	θ_3
4	$\pi/2$	0	d_4 (0.10915 m)	$\theta_4 - \pi/2$
5	$-\pi/2$	0	d_5 (0.09456 m)	θ_5
6	0	0	d_6 (0.0823 m)	θ_6

Back-propagation Through Time algorithm is used to validate the torque error compensation capability of the proposed deep neural network architecture.

IV. EXPERIMENTAL VERIFICATION

A. EXPERIMENTAL PLATFORM

UR5 is a human-robot collaborative robot with six rotating joints; Figure 4 shows its real structure and the link coordinate system. We define the position variable of joint i is θ_i. Table 1 gives the specifications of the links and the D-H coordinate system. The range of every joint rotation angle of UR5 is $[-360, 360]$ (unit: deg), and every joint acceleration range is [0, 180] (unit: deg/s^2). The UR5 is very popular in robot research, but the manufacturer has not publicly provided researchers with a complete and reliable dynamic model and its specific parameters. Unfortunately, the established dynamic model and identified parameters values of UR5 have not been found in the existing study, it is not straightforward to learn the research results.

B. SYMBOLIZATION OF BASIC PARAMETERS

The dynamic parameters of an industrial robot can be classified into three groups: unidentifiable, identifiable parameters in linear combinations, and fully identifiable. Since the dynamics parameters are redundant to determine the manipulator dynamic model uniquely, it is impossible to estimate all the dynamic parameters value of a robot [27]. Besides, when the observation matrix is not often a full-rank matrix, the solution of the least squares method is not unique. The minimum inertia parameter is the only identifiable parameter, and the use of basic inertia parameters in the Newton-Euler dynamics algorithm can effectively reduce calculations. UR5 has 72 parameters in total, and 48 identifiable parameters are obtained by eliminating the unidentifiable parameters and reorganizing them. Table 2 lists the minimum parameter set of the UR5, where the "—" are the unidentifiable parameters, and Table 3 gives the symbolic expressions of restructured parameters.

C. DATA COLLECTION AND PROCESSING

According to the classification of the robot's link weight, the three links with large self-weight are called the first three links, and the three links with small self-weight are called the last three links. The step-by-step identification method can effectively improve the identification accuracy of the last three links [28]. Assume the sampling frequency of the joint state is w_s and the fundamental frequency of the trajectories is w_f, the collected samples over one period is w_s/w_f. In both identification experiments, we operated the manipulator to execute eight times according to the reference trajectory and collect the data synchronously. We chose the fundamental frequency w_f of the step-by-step excitation trajectory as 2/65 Hz and 1/30 Hz, respectively. In addition, we collected the joint position, velocity, and current information at a sampling frequency w_s of 100 Hz and obtained 3,250 samples and 3,000 samples respectively. According to (13), the time-domain average processing is performed on the collected data to improve the accuracy of the sampled data.

The measurements of position $\hat{\boldsymbol{q}}$ and velocity $\hat{\dot{\boldsymbol{q}}}$ were processed with forward and reverse IIR Butterworth filters, using 10 Hz cut-off low-pass frequency. The joint acceleration $\hat{\ddot{\boldsymbol{q}}}$ was calculated by using a central difference algorithm.

The motor current of each joint is multiplied with the motor torque constant and gear ratio, and RLOESS analysis processing using the smooth function of MATLAB to obtain the torque of each joint of the UR5. In terms of physical parameters: motor torque constant is $K_i = 0.125Nm/A, i = 1, \cdots, 3$; $K_i = 0.0922Nm/A, i = 4, \cdots, 6$; gear ratio: $R_i = 101, i = 1, \cdots, 6$.

D. PARAMETERS ESTIMATION

Based on the experimental data and the identification model of robot inverse dynamics, we performed parameter identification of the UR5. Increasing the number of sampling points of the observation matrix of the inverse dynamics identification equation can effectively improve the identification accuracy. According to the description in Section II.B, the least squares method is used for numerical identification of dynamic parameters. $\hat{\beta}$ is the identification value of the basic inertia parameter; $\sigma_{\hat{\beta}_{jr}}$ % is the relative standard deviation of the identified value, the smaller the value of the relative standard deviation, the more accurate the identification

TABLE 2. Simplified base inertial parameters of UR5 robot, where the "—" are the unidentifiable parameters.

Joint #	XX_i	XY_i	XZ_i	YY_i	YZ_i	ZZ_i	MX_i	MY_i	MZ_i	M_i	f_{vi}	f_{ci}
Joint 1	—	—	—	YYR_1	—	—	—	—	—	—	f_{v1}	f_{c1}
Joint 2	XXR_2	XY_2	XZR_2	—	YZ_2	ZZR_2	MXR_2	MY_2	—	—	f_{v2}	f_{c2}
Joint 3	XXR_3	XY_3	XZR_3	—	YZ_3	ZZR_3	MXR_3	MY_3	—	—	f_{v3}	f_{c3}
Joint 4	XXR_4	XY_4	XZ_4	YYR_4	YZ_4	—	MX_4	—	MZR_4	—	f_{v4}	f_{c4}
Joint 5	XXR_5	XY_5	XZ_5	YYR_5	YZ_5	—	MX_5	—	MZR_5	—	f_{v5}	f_{c5}
Joint 6	XXR_6	XY_6	XZ_6	—	YZ_6	ZZ_6	MX_6	MY_6	—	—	f_{v6}	f_{c6}

TABLE 3. Symbolic expressions of restructured parameters.

Link 1:
$YYR_1=YY_1+YY_2+YY_3+ZZ_4+0.2183*MY_4-0.180625*M_2-0.3344850625*M_3-0.32257134*(M_4+M_5+M_6)$
Link 2:
$XXR_2=XX_2-YY_2+0.180625*(M_2+M_3+M_4+M_5+M_6)$
$XZR_2=XZ_2-0.425*(MZ_2+MZ_3+MY_4)-0.04638875*(M_4+M_5+M_6)$
$ZZR_2=ZZ_2-0.180625*(M_2+M_3+M_4+M_5+M_6)$
$MXR_2=MX_2+0.425*(M_2+M_3+M_4+M_5+M_6)$
Link 3:
$XXR_3=XX_3-YY_3+0.1538600625*(M_3+M_4+M_5+M_6)$
$XZR_3=XZ_3-0.39225*(MZ_3+MY_4)-0.0428140875*(M_4+M_5+M_6)$
$ZZR_3=ZZ_3-0.1538600625*(M_3+M_4+M_5+M_6)$
$MXR_3=MX_3+0.39225*(M_3+M_4+M_5+M_6)$
Link 4:
$XXR_4=XX_4-ZZ_4+ZZ_5-0.18912*MY_5+0.089415936*(M_5+M_6)$
$YYR_4=YY_4+ZZ_5-0.18912*MY_5+0.089415936*(M_5+M_6)$
$MZR_4=MZ_4-MY_5+0.09456*(M_5+M_6)$
Link 5:
$XXR_5=XX_5-ZZ_5+YY_6+0.1646*MZ_6+0.00677329*M_6$
$YYR_5=YY_5+YY_6+0.1646*MZ_6+0.00677329*M_6$
$MZR_5=MZ_5+MZ6+0.0823*M_6$
Link 6:
$XXR_6=XX_6-YY_6$

result. Table 4 lists parameter identification values and relative standard deviations.

Figure 5 shows the predicted torques of the physical model and real torques and their errors. The black line is the measured torque, the red dotted line is the predicted torque of the physical model, and the blue dotted line is the error. The root mean square error (RMSE) of the measured torque τ_m and the predicted torque τ_p of the identified trajectory is calculated to verify the deviation of the predicted torque. The RMSE is defined as follows:

$$RMSE = \sqrt{\frac{1}{K}\sum_{k}^{K}(\tau_{m,k} - \tau_{p,k})^2} \tag{25}$$

where $\tau_{m,k}$ is the actual torque value of the k^{th} point, $\tau_{p,k}$ is the k^{th} predicted torque point, K is the total number of measurement data. According to the calculation of experimental data, the RMSE of the identification trajectory of joints 1, 2, 3 is 2.763 Nm, 2.843 Nm, 2.575 Nm, the RMSE of the identification trajectory of joints 4, 5, 6 is 0.307 Nm, 0.408 Nm and 0.407 Nm, respectively.

E. PROPOSED UNCERTAINTY COMPENSATION MODEL VERIFICATION

In this section, we focus on verifying the performance of the proposed deep learning model architecture based on LSTM and attention mechanism in robot uncertainties compensation. First, to demonstrate the proposed approach robustness, we compare it with the shallow fully-connected neural networks model. Then, we show how the proposed model for predict torque compensation can be enhanced by the influence of (1) valid input, (2) the timestep and (3) the attention mechanism.

To capture rich non-linear relationships, a large number of samples are needed as the data support for training deep learning networks [29]. In an ideal case, the dataset contains all possible motion conditions of the robot. However, due to

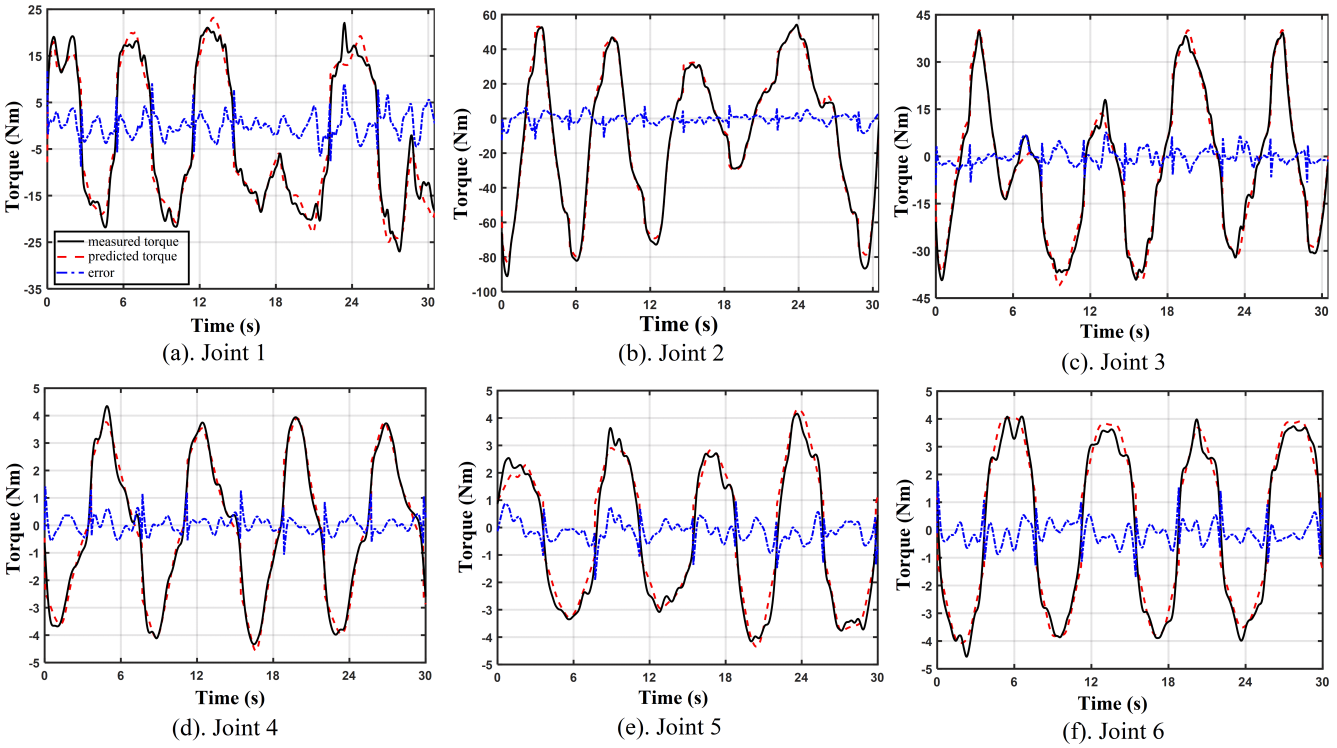

FIGURE 5. The comparison of predicted and measured torques with the given identification trajectory.

the high-dimensional state space in which the robot motion, it is often impossible to obtain such a rich data set. Shareef *et al.* selected eleven parameterized sine trajectories in the model space for independent joint learning of robot inverse dynamics [30]. Peter *et al.* proposed training a large number of different trajectories to increase the generalization ability of the model [31].'

According to the robot's rotation angle and installation restrictions, the selected robot workspace is a hemisphere with an approximate radius of 850 mm above the installation plane; Table 5 lists the range of joint motion. We chose 1,000 points in the selected robot workspace in a rhythmic, discontinuous motion method to make it close to the actual working conditions. The joint speed range is 2.0-3.0 rad/s, the acceleration range is 2.2-3.0 rad/s^2, the selection range of joint speed and acceleration covers the high-speed operating requirements of the robot. The distribution of training samples in the system state space and data processing methods impact on the generalization ability of the network. Features that cannot be learned must be eliminated, such as noise and high-frequency vibrations; otherwise, the learning of basic features will be disturbed, and accuracy will be reduced. We collected the position, speed, and current information of the robot at a frequency of 60 Hz. A total of 154440 valid samples were obtained as the training data set after sign process consistent with the identification procedure. According to a ratio of 80% −20% [22], we divided the sample data into a training set and a test set for deep learning cross-training. Each sample of the training and test dataset contains 24 pieces of information: eighteen input data (six joint positions, six joint speeds, and six joint accelerations of manipulator), and six output data (six torque errors of manipulator). When input data participates in model training, the input data is selected by the ICM. All input and output data are normalized to perform proportional scaling to improve model accuracy and convergence speed. The normalized formula is as follows:

$$x_R = \frac{x_r - x_{min}}{x_{max} - x_{min}} \tag{26}$$

where x_r is the true value of the data, x_{min} and x_{max} are the minimum and maximum values in the data, x_R is the normalized value.

We compared the network with three fully-connected layers and three-layer network one of which is LSTM to verify the superiority of LSTM in predicting dynamic time series data. The ICM determines the number of input layer nodes, and one output data, which is predict error of target joint, determines the number of output layer node. We changed the number of nodes of a single hidden layer to prove the capability of the neural network and LSTM and its evaluation index is the RMSE of target joint error. Figure 6 shows the prediction ability of the fully-connected neural network and LSTM of joint 1. As the number of nodes in the hidden layer increases, the RMSE of the three fully-connected layers is decreasing and the RMSE of three-layer network with LSTM declined first and then stabilized. Overall, when using different hidden node to predict the performance of fully-connected network and LSTM, the torque compensation effect of the

TABLE 4. The values of estimated base parameters of UR5.

Parameters	$\hat{\beta}$	$\sigma_{\hat{\beta}_{jr}}\%$
$YYR_1\,(Kg{\cdot}m^2)$	8.3761	0.2985
$f_{v1}\,(Nm/rad{\cdot}s^{-1})$	11.6400	0.3276
$f_{c1}\,(Nm/rad{\cdot}s^{-1})$	7.9027	0.3333
$XXR_2\,(Kg{\cdot}m^2)$	-5.2958	0.4344
$XY_2\,(Kg{\cdot}m^2)$	-0.4263	2.6580
$XZR_2\,(Kg{\cdot}m^2)$	0.3516	3.8198
$YZ_2\,(Kg{\cdot}m^2)$	-0.4040	3.0481
$ZZR_2\,(Kg{\cdot}m^2)$	6.8123	0.3516
$MXR_2\,(Kg{\cdot}m^2)$	-4.2925	0.0769
$MY_2\,(Kg{\cdot}m^2)$	0.0285	1.3105
$f_{v2}\,(Nm/rad{\cdot}s^{-1})$	9.7274	0.3004
$f_{c2}\,(Nm/rad{\cdot}s^{-1})$	8.0567	0.3109
$XXR_3\,(Kg{\cdot}m^2)$	-3.2231	0.5960
$XY_3\,(Kg{\cdot}m^2)$	-0.2807	3.7101
$XZR_3\,(Kg{\cdot}m^2)$	-0.1922	6.0187
$YZ_3\,(Kg{\cdot}m^2)$	-0.8108	1.1181
$ZZR_3\,(Kg{\cdot}m^2)$	3.1272	0.3813
$MXR_3\,(Kg{\cdot}m^2)$	-1.9423	0.0934
$MY_3\,(Kg{\cdot}m^2)$	-0.0039	3.2954
$f_{v3}\,(Nm/rad{\cdot}s^{-1})$	10.1556	0.2201
$f_{c3}\,(Nm/rad{\cdot}s^{-1})$	7.6093	0.3283
$XXR_4\,(Kg{\cdot}m^2)$	0.3584	16.3031
$XY_4\,(Kg{\cdot}m^2)$	-0.0442	11.8178
$XZ_4\,(Kg{\cdot}m^2)$	0.1253	10.2596
$YYR_4\,(Kg{\cdot}m^2)$	0.1043	9.4785
$YZ_4\,(Kg{\cdot}m^2)$	0.0101	7.6555
$MX_4\,(Kg{\cdot}m^2)$	-0.1628	1.0162
$MZR_4\,(Kg{\cdot}m^2)$	0.0120	8.8995
$f_{v4}\,(Nm/rad{\cdot}s^{-1})$	1.2254	0.8778
$f_{c4}\,(Nm/rad{\cdot}s^{-1})$	0.9957	1.0959
$XXR_5\,(Kg{\cdot}m^2)$	-0.0634	8.9245
$XY_5\,(Kg{\cdot}m^2)$	0.0488	6.8208
$XZ_5\,(Kg{\cdot}m^2)$	0.0235	9.9913
$YYR_5\,(Kg{\cdot}m^2)$	-0.0674	9.1760
$YZ_5\,(Kg{\cdot}m^2)$	0.0770	4.6326
$MX_5\,(Kg{\cdot}m^2)$	0.0105	5.2102
$MZR_5\,(Kg{\cdot}m^2)$	-0.0224	3.9341
$f_{v5}\,(Nm/rad{\cdot}s^{-1})$	1.6281	0.6305
$f_{c5}\,(Nm/rad{\cdot}s^{-1})$	0.9646	1.0240
$XXR_6\,(Kg{\cdot}m^2)$	-0.0099	9.4475
$XY_6\,(Kg{\cdot}m^2)$	-0.0033	14.8924
$XZ_6\,(Kg{\cdot}m^2)$	-0.0163	7.3671
$YZ_6\,(Kg{\cdot}m^2)$	0.0098	12.5876
$ZZ_6\,(Kg{\cdot}m^2)$	-0.0582	7.5107
$MX_6\,(Kg{\cdot}m^2)$	-0.0044	7.1986
$MY_6\,(Kg{\cdot}m^2)$	-0.0005	5.9947
$f_{v6}\,(Nm/rad{\cdot}s^{-1})$	1.3392	0.6302
$f_{c6}\,(Nm/rad{\cdot}s^{-1})$	1.2096	0.9172

former is always worse than the latter. Here, we only give the comparison results of joint 1 and the performance of other joints is similar, that is the performance of the LSTM is better than the full-connected shallow neural network in predicting time series data, we do not repeat the description.

TABLE 5. Rotation range of each joint in the selected robot workspace.

Joint #	Joint 1	Joint 2	Joint 3
range of motion (*deg*)	[-180,180]	[-180,0]	[-130,130]
Joint #	Joint 4	Joint 5	Joint 6
range of motion (*deg*)	[-180,0]	[-180,180]	[-180,180]

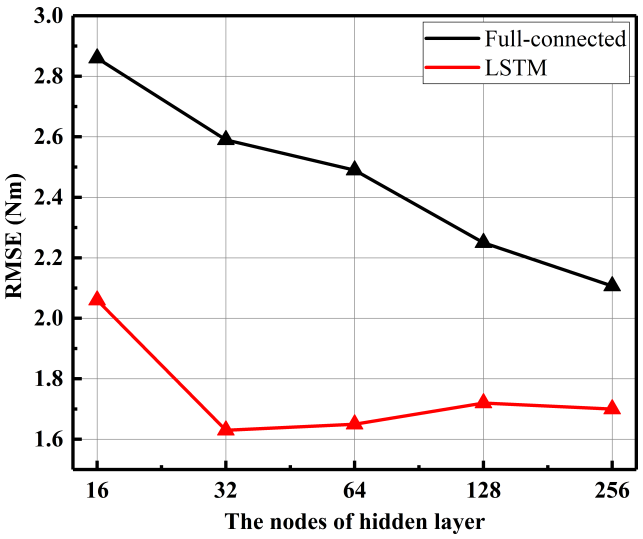

FIGURE 6. The prediction ability of the full-connected neural network and LSTM of joint 1.

We used 5-fold cross-validation to verify the proposed deep learning architecture for uncertainty compensation. The method divides the sample data into five parts, turns four of them into training data, and takes the remaining one as test data. The average of the five predicted results of the test set is used as a performance indicator of model prediction accuracy to achieve the purpose of making full use of the data and making the experimental results objective. We changed the valid input, timestep and network structure to examine the performance of the proposed network, and the RMSE of the torque prediction of the test set is used as a criterion for evaluating the training network ability. The number of LSTM nodes in the encoder layer and the re-encoder layer are both 128, Solver Adam [32] was used to optimize the loss function, the learning rate was 0.05, and the dropout [33] value was 0.5. We chose the hyper-parameters with which the model performed best. We train the network by changing the number of valid input (e.g., input after ICM, three input for each joint, and eighteen input for each joint) and the timestep (e.g., 2,3,5 and 10) to get the greater parameters by comparing the training results of different variable. Figure 7 shows the predicted results of six joints of the test set, which reflects the impact of changes of valid input and timestep on the performance of the proposed UCM.

In the five-fold cross-validation, the torque errors of the selected test set without torque compensation are 3.112 Nm, 2.958 Nm, 2.633 Nm, 0.417 Nm, 0.457 Nm and 0.444 Nm,

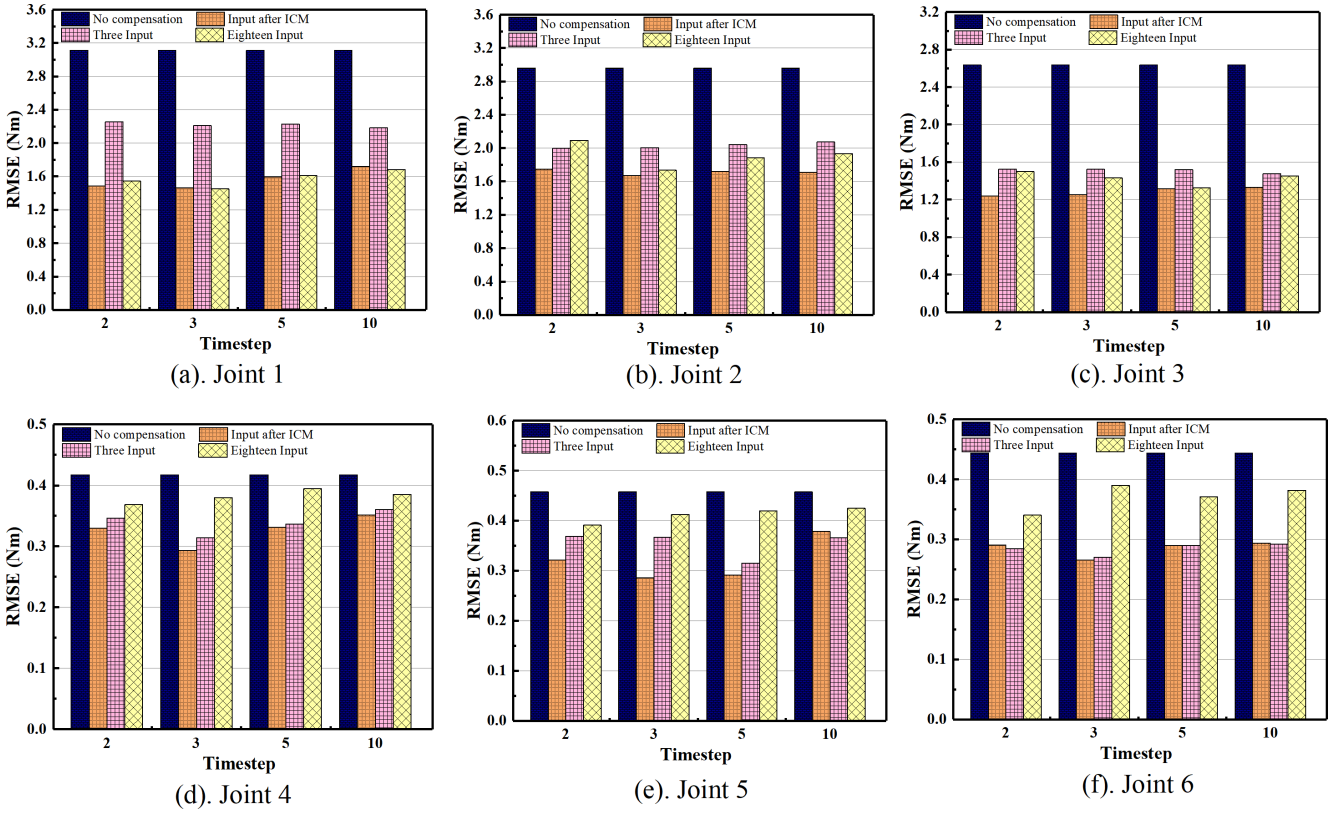

FIGURE 7. The impact of changes of valid input and timestep on the performance of the proposed UCM.

respectively for six joint, which is the highest bar in Figure 8. Relatively, after compensated by the optimal model, which contains an attention mechanism, the timestep is 3, and the input data is processed by ICM, the torque errors of the six joints are 1.463 Nm, 1.671 Nm, 1.253 Nm, 0.293 Nm, 0.286 Nm and 0.265 Nm, respectively, which are shown in Table 6. The experiments verified: (1) Compared with training result of input after processing of ICM, the RMSE of each joint with eighteen input gradually increases from joint 1 to joint 6. Also, compared with input after ICM, the RMSE of each joint with three input gradually decreases from joint 1 to joint 6. The training results of the input data after ICM have the best performance. The above phenomenon shows that as the joints 1, 2, …, 6 gradually away from the pedestal of tandem manipulator, the effective input for compensation model training gradually decreases. For the first joint close to the pedestal, the performance is best when the input is 18 and the input is from the ICM (the above two inputs actually are the same), and the worst is when the input is 3. However, for the sixth joint away from the pedestal, the performance is best when the input is 3 and the input is from ICM (in fact, the two input are the same), and the performance is the worst when the input is 18. The result of the above comparison is an effective verification of the proposed ICM theory. (2) Participating in model training with multiple timesteps obtain rich data features from different timestep data. However, when the timestep exceeds a certain length, long-distance memory loss will occur. We set the timestep size to 2, 3, 5, and 10 for model training to examine the effect of timestep on the proposed model performance. The experimental results show that the training effect is better when the time step is 3, which shows that the compensation model with a timestep of 3 has a stronger ability to capture the information features of the sequence, and when the timestep is too long, information loss occur. (3) The proposed UCM to aid the manipulator's torque error compensation has good results, which effectively reduces the deviation between the predicted torque and the real torque, and the specific error features that the model can capture will be verified in the next section.

Besides, there are differences in the importance of features in short subsequences of long sequences, and important salient features often contain more information. If the LSTM is given the ability to pay attention to important features, it can better achieve the effective extraction of short-term models and the optimization of input information. We chose the network structure with the best performance to verify the superiority of the attention mechanism by comparing the deep network with or without attention mechanism. Experimental results are given in Table 6, which indicates that the model with attention mechanism has a better ability to capture data features and improve prediction effect.

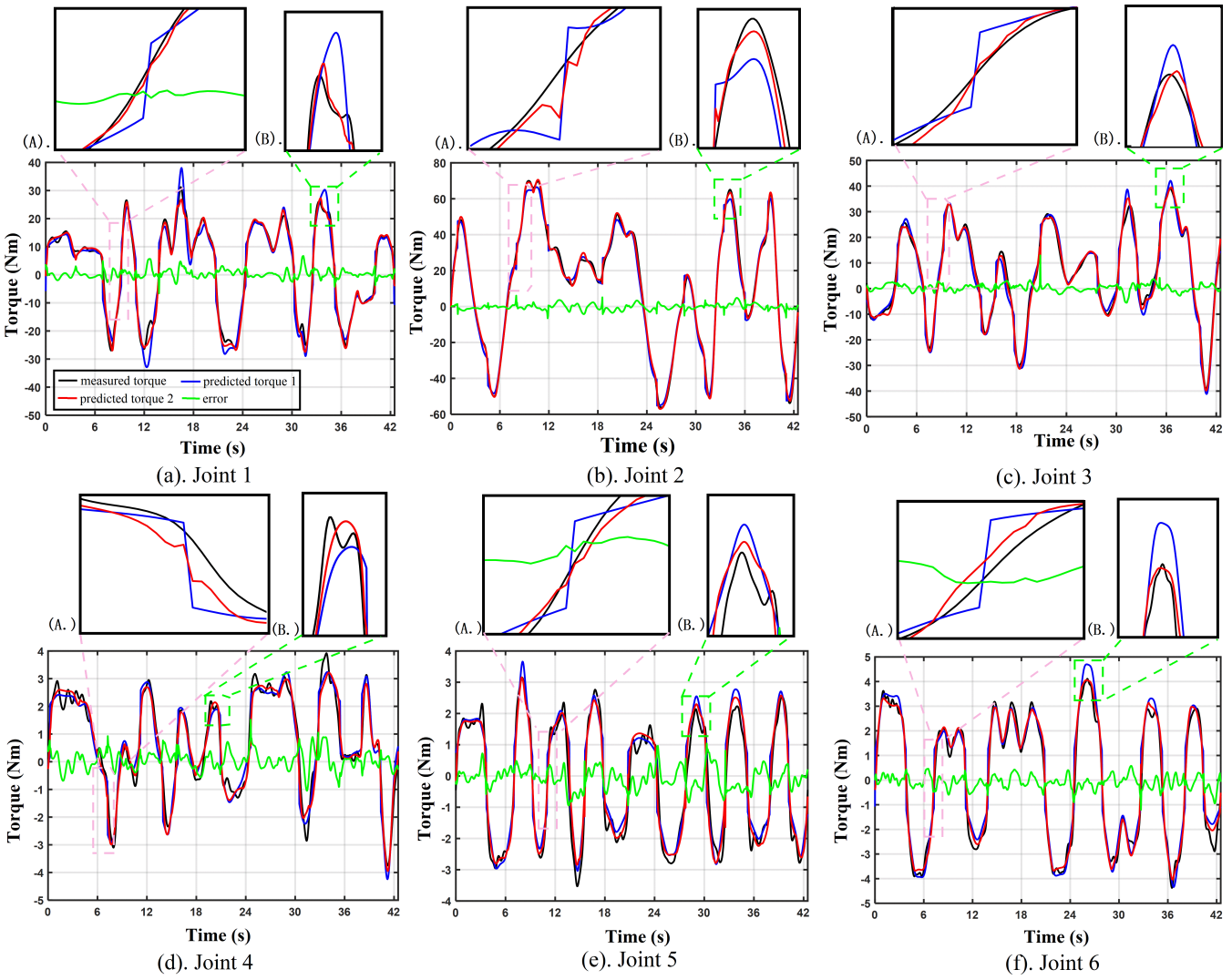

FIGURE 8. The comparison of the measured torques, predicted torques by physical model called predicted torque 1 and compensated torques of physical model called predicted torque 2 with the verified trajectory.

TABLE 6. Uncompensated RMSE and whether the optimal model with attention mechanism compensated RMSE of the test set. (units: Nm).

Joint #	Physical model	With attention	No attention
Joint 1	3.112	1.463	1.670
Joint 2	2.958	1.671	1.715
Joint 3	2.633	1.253	1.274
Joint 4	0.417	0.293	0.342
Joint 5	0.457	0.286	0.326
Joint 6	0.444	0.265	0.291

In conclusion, experiments show, LSTM-based deep learning architecture performs better than shallow neural networks in predicting accuracy, proving the time series characteristics of dynamics are more suitable for prediction with LSTM. The predicted accuracy is distinct when the selected training set and test set are different, which shows that it is necessary to increase the objectivity of predicted results through cross-training. Also, the selection of effective input data avoids the model unnecessary interference and improves the accuracy of model prediction. Then, a reasonable timestep can improve the ability to capture data features and avoid remote memory loss. Moreover, the attention mechanism achieves an efficient allocation of data resources, highlights important features in the data, and enhances the model's capabilities.

F. TRAJECTORY VERIFICATION OF THE PROPOSED UNCERTAINTY COMPENSATION METHOD

We designed a new trajectory different from the identification trajectory [12] to verify the results of robot dynamic parameter identification and the effect of the proposed UCM. The verification trajectory ran at high-speed state with a speed range of 2.0-3.0 rad/s, the working time is 42.5 s, and the sampling frequency is 100 Hz. Figure 8 compares the measured torques, predicted torques by physical model called predicted torque 1 in figure and compensated torques of physical model called predicted torque 2 in figure with the

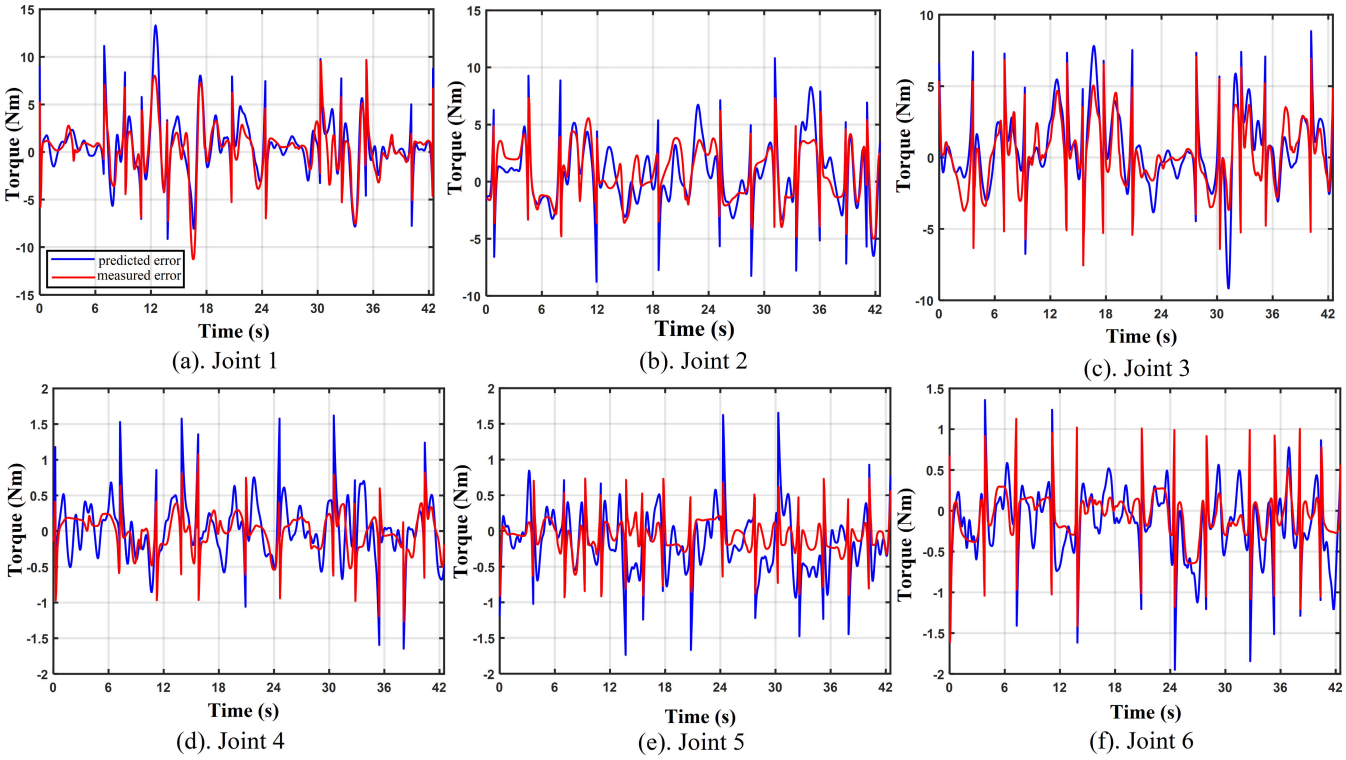

FIGURE 9. The comparison of measured errors between predicted torques calculated by physical dynamic model and measured torques and predicted errors after the UCM of verified trajectory.

verified trajectory. The black, blue, red lines are the above torque representation respectively and the green line denotes error of between measured torque and predicted torque 2, meanwhile, parts (A.) and (B.) of each joint are enlarged area of the torque comparison graph. We verified the identification result by the relative error percentage of the verification trajectory, which is defined as:

$$\varepsilon_r = \frac{\|\tau_m - \tau_p\|}{\|\tau_m\|} \times 100\% \tag{27}$$

where τ_m is the actual torque, τ_p represents the predicted torque of the physical dynamic model.

Table 7 summarizes the relative error percentage of the identification trajectory torque and the verification trajectory torque. As shown, both solutions present values of relative error identified for identification trajectory are less than 8%, and the relative error of the verified trajectory is 8.84%, which proves the good identification parameter value [34]. Meanwhile, the relative error percentage of the verified trajectory after compensation is only 4.75%, which is significantly lower than 8.84% of the trajectory without error compensation, which proves that the proposed uncertainty compensation method has a good performance.

TABLE 7. Percentage of relative errors of predicted torques for identification and validation trajectories.

Trajectories	ε_r (%)
Identification trajectory – joint 1, 2, 3	7.56
Identification trajectory – joint 4, 5, 6	7.78
Validation trajectory	8.84
Validation after compensation	4.75

Under the premise of accurate modeling of dynamics, there always be errors due to the uncertainties that include unmodeled factors and the inaccuracy of the identification parameters. There are two main reasons of the torque tracking error of the physical model: (1) Friction is a particularly complex non-linear phenomenon, and accurate modeling for its characteristics has always been a problem in high-quality motion control, which cause the peak of error due to waveform distortion when the joint velocity passes through zero, for example, this phenomenon is shown in [5], [12]. The design of the friction compensation algorithm is of great significance to improve the robot's motion performance; (2) The tracking error of local maximum torque occurs when the joint acceleration crosses zero. Due to the large change of the joint inertia and the strong coupling at high speed, the uncertainty error is obvious, and the error of local maximum torque is particularly significant.

The proposed UCM has a good ability to capture the physical effect of the error peak caused by friction, specifically, the image of in the verified trajectory has an area where the friction compensation phenomena is magnified and shown in part (A.) of each joint of Figure 8. The blue line in part (A.) represent the inadequate modeling of friction in the physical dynamics model, which is the inherent defect of physical

TABLE 8. The RMSE of the only physical model and after torque compensation. (units: Nm).

Joint #	Max Torque (MT)	RMSE of the Physical Model	Percentage of MT (%)	RMSE after Compensation	Percentage of MT (%)
Joint 1	40	3.149	7.87	1.541	3.85
Joint 2	70	2.937	4.20	1.735	2.47
Joint 3	40	2.621	6.55	1.431	3.58
Joint 4	5	0.421	8.42	0.293	5.86
Joint 5	5	0.458	9.16	0.289	5.78
Joint 6	5	0.453	9.06	0.262	5.24

model and leads to inevitable sudden torque changes when the joint changes direction. Meanwhile, the effect of local maximum torque error caused by the strong coupling in high-speed motion when the joint's acceleration crosses zero is shown in (B.) of each joint of Figure 8. The other compensation parts of friction and error of local maximum torque in the figure are similar to the effect of the enlargement. And, Figure 9 shows the measured error and predicted error, where the predicted errors calculated by the proposed UCM are shown using the red line, the blue line represent the measured errors between predicted torques calculated by the physical dynamic model and measured torques. It can be seen that the proposed UCM model has a good performance in compensating friction and local maximum torque errors. In detail, when the joint changes direction, the torque mutation after compensation (red line in part (A.)) becomes small or disappears, which makes predicted torque after compensation closer to the measured torque (black line in part (A.)). Moreover, the proposed method makes the compensated predicted torque (red line in part (B.)) close to the real torque (black line in part (B.)) at the local maximum torque. However, comparing with the first three joints, some degradation occurs owing to smaller torque and error values, since inertial parameters are relatively small and the insignificant change in error value makes the error feature more difficult to capture than the first three links with large weight. The specific evaluation is reflected in Table 8, which represents the RMSE of each joint and the percentage of error torque in the maximum torque of the verification trajectory. It can be inferred that for the first three joints the RMSE after compensation are below 2 Nm, they account for about 3% of the maximum torque, which has an outstanding torque tracking effect than the 7% before compensation. For the last three joints, the RMSE after compensation are below 0.3 Nm, which size about 5% of the maximum torque and perform better than 9% before compensation. Overall, the compensation effect is obvious and the above results verified the effectiveness of the proposed method in considering uncertainties and improved the accuracy of torque prediction.

V. CONCLUSION

In order to obtain accurately predicted torque, this article applies deep learning for the first time to aid robot dynamic parameter identification of 6 degrees of freedom robot manipulator for compensation of uncertain factors, which is the source of robot torque tracking error. We introduced a robust and generic uncertainty compensation model that relies on proposed Input Control Module (ICM), Error Learning Models (ELMs) based on Long-Short-Term Memory and attention mechanism, which is able to perform well on solving the main problem of robot torque error, specifically, that is the difficulty of capturing the friction characteristics and compensating the error of local maximum torques. The proposed ICM can select valid input and reduce the unnecessary interference for ELMs. And, the ELMs, consisted by ELM units, concern establishing the mapping of the motion feature and joint torque deviation to compensate the joint error. Moreover, we summarized the effects of valid input, the timestep and attention mechanism on the performance of the proposed compensation model. We launched an experiment on the UR5 manipulator and published the reference values of its identifiable dynamic parameters. Meanwhile, we carried out a comprehensive evaluation of the verification trajectories of six joints, which prove the reliability of identified parameters and the validity of above proposed models. Overall, our experimental results have shown the robustness and effectiveness of the proposed method for uncertainty compensation.

REFERENCES

[1] W. Wu, S. Zhu, X. Wang, and H. Liu, "Closed-loop dynamic parameter identification of robot manipulators using modified Fourier series," *Int. J. Adv. Robot. Syst.*, vol. 9, no. 1, p. 29, Mar. 2012.

[2] A. Jubien, M. Gautier, and A. Janot, "Dynamic identification of the kuka LightWeight robot: Comparison between actual and confidential Kuka's parameters," in *Proc. IEEE/ASME Int. Conf. Adv. Intell. Mechatronics*, Besancon, France, Jul. 2014, pp. 483–488.

[3] K. Radkhah, D. Kulic, and E. Croft, "Dynamic parameter identification for the CRS A460 robot," in *Proc. IEEE/RSJ Int. Conf. Intell. Robots Syst.*, San Diego, CA, USA, Oct. 2007, pp. 3842–3847.

[4] M. Gautier, "Dynamic identification of robots with power model," in *Proc. Int. Conf. Robot. Autom.*, Albuquerque, NM, USA, Apr. 1997, pp. 1922–1927.

[5] J. Jin and N. Gans, "Parameter identification for industrial robots with a fast and robust trajectory design approach," *Robot. Comput.-Integr. Manuf.*, vol. 31, pp. 21–29, Feb. 2015.

[6] H. P. Ni, C. R. Zhang, T. L. Hu, T. Wang, Q. Z. Chen, and C. Chen, "A dynamic parameter identification method of industrial robots considering joint elasticity," *Int. J. Adv. Robot. Syst.*, vol. 16, no. 1, Feb. 2019, Art. no. 1729881418825217.

[7] C. G. Atkeson, C. H. An, and J. M. Hollerbach, "Estimation of inertial parameters of manipulator loads and links," in *Proc. 3rd Int. Symp. Robot. Res.*, Gouvieux, FR, USA, 1986, pp. 221–228.

[8] K.-J. Park, "Fourier-based optimal excitation trajectories for the dynamic identification of robots," *Robotica*, vol. 24, no. 5, pp. 625–633, Sep. 2006.

[9] J. Swevers, C. Ganseman, D. B. Tukel, J. de Schutter, and H. Van Brussel, "Optimal robot excitation and identification," *IEEE Trans. Robot. Autom.*, vol. 13, no. 5, pp. 730–740, Oct. 1997.

[10] G. Calafiore, M. Indri, and B. Bona, "Robot dynamic calibration: Optimal excitation trajectories and experimental parameter estimation," *J. Robot. Syst.*, vol. 18, no. 2, pp. 55–68, 2001.
[11] M. Gautier and W. Khalil, "Direct calculation of minimum set of inertial parameters of serial robots," *IEEE Trans. Robot. Autom.*, vol. 6, no. 3, pp. 368–373, Jun. 1990.
[12] S. Jiang, M. Jiang, Y. Cao, D. Hua, H. Wu, Y. Ding, and B. Chen, "A typical dynamic parameter identification method of 6-degree-of-freedom industrial robot," *Proc. Inst. Mech. Eng., I, J. Syst. Control Eng.*, vol. 231, no. 9, pp. 740–752, Oct. 2017.
[13] W. Ge, B. Wang, and H. Mu, "Dynamic parameter identification for reconfigurable robot using adaline neural network," in *Proc. IEEE Int. Conf. Mechatronics Autom. (ICMA)*, Tianjin, China, Aug. 2019, pp. 319–324.
[14] A. S. Polydoros, E. Boukas, and L. Nalpantidis, "Online multi-target learning of inverse dynamics models for computed-torque control of compliant manipulators," in *Proc. IEEE/RSJ Int. Conf. Intell. Robot. Syst. (IROS)*, Vancouver, BC, Canada, Sep. 2017, pp. 4716–4722.
[15] M. N. Duc and T. N. Trong, "Neural network structures for identification of nonlinear dynamic robotic manipulator," in *Proc. IEEE Int. Conf. Mechatronics Autom.*, Tianjin, China, Aug. 2014, pp. 1575–1580.
[16] V. Bargsten, J. De Gea Fernandez, and Y. Kassahun, "Experimental robot inverse dynamics identification using classical and machine learning techniques," in *Proc. 47th Int. Symp. Robot.*, Munich, Germany, Jun. 2016, pp. 17–22.
[17] B. Liang, T. Li, Z. Chen, Y. Wang, and Y. Liao, "Robot arm dynamics control based on deep learning and physical simulation," in *Proc. 37th Chin. Control Conf. (CCC)*, Wuhan, China, Jul. 2018, pp. 2921–2925.
[18] Y. Hua, Z. Zhao, R. Li, X. Chen, Z. Liu, and H. Zhang, "Deep learning with long short-term memory for time series prediction," *IEEE Commun. Mag.*, vol. 57, no. 6, pp. 114–119, Jun. 2019.
[19] D. Furuta, K. Kutsuzawa, S. Sakaino, and T. Tsuji, "LSTM learning of inverse dynamics with contact in various environments," in *Proc. 10th Eur.-Asia Congr. Mechatronics*, Tsu, Japan, Sep. 2018, pp. 149–154.
[20] J. Schmidhuber, "Deep learning in neural networks: An overview," *Neural Netw.*, vol. 61, pp. 85–117, Jan. 2015.
[21] N. Liu, L. Li, B. Hao, L. Yang, T. Hu, T. Xue, and S. Wang, "Modeling and simulation of robot inverse dynamics using LSTM-based deep learning algorithm for smart cities and factories," *IEEE Access*, vol. 7, pp. 173989–173998, 2019.
[22] R. Mukhopadhyay, R. Chaki, A. Sutradhar, and P. Chattopadhyay, "Model Learning for Robotic Manipulators using Recurrent Neural Networks," in *Proc. IEEE Region Conf., Technol.*, Kerala, India, Oct. 2019, pp. 2251–2256.
[23] M. Gautier and W. Khalil, "Identification of the minimum inertial parameters of robots," in *Proc. Int. Conf. Robot. Autom.*, Scottsdale, AZ, USA, 1989, pp. 1529–1534.
[24] Z. Qin, L. Baron, and L. Birglen, "A new approach to the dynamic parameter identification of robotic manipulators," *Robotica*, vol. 28, no. 4, pp. 539–547, Jul. 2010.
[25] W. Khalil and E. Dombre, "Identification of the dynamic parameters-identification of the dynamic parameters," in *Proc. Modeling Identificat. Control Robot.*, 2004, pp. 291–311.
[26] A. Vaswani, "Attention is all you need," in *Proc. 31st Annu. Conf. Neural Inf. Process. Syst.*, Long Beach, CA, USA, Dec. 2017, pp. 5999–6009.
[27] J. Wu, J. Wang, and Z. You, "An overview of dynamic parameter identification of robots," *Robot. Comput.-Integr. Manuf.*, vol. 26, no. 5, pp. 414–419, Oct. 2010.
[28] J. Xiao, F. Zeng, Q. Zhang, and H. Liu, "Research on the forcefree control of cooperative robots based on dynamic parameters identification," *Ind. Robots. Int. J. Robot. Res. Appl.*, vol. 46, no. 4, pp. 499–509, Jun. 2019.
[29] O. Sigaud, C. Salaün, and V. Padois, "On-line regression algorithms for learning mechanical models of robots: A survey," *Robot. Auto. Syst.*, vol. 59, no. 12, pp. 1115–1129, Dec. 2011.
[30] Z. Shareef, F. Reinhart, and J. Steil, "Generalizing a learned inverse dynamic model of KUKA LWR IV+ for load variations using regression in the model space," in *Proc. IEEE/RSJ Int. Conf. Intell. Robots Syst. (IROS)*, Daejeon, South Korea, Oct. 2016, pp. 606–611.
[31] H. C. Nho and P. Meckl, "Intelligent feedforward control and payload estimation for a two-link robotic manipulator," *IEEE/ASME Trans. Mechatronics*, vol. 8, no. 2, pp. 277–283, Jun. 2003.
[32] D. P. Kingma and J. L. Ba, "Adam: A method for stochastic optimization," in *Proc. 3rd Int. Conf. Learn. Represent.*, San Diego, CA, USA, May 2015, pp. 1–4.
[33] Y. Gal and Z. Ghahramani, "Dropout as a Bayesian approximation: Representing model uncertainty in deep learning," in *Proc. 33rd Int. Conf. Mach. Learn.*, New York, NY, USA, Jun. 2016, pp. 1651–1660.
[34] C. D. Sousa and R. Cortesáo, "Physical feasibility of robot base inertial parameter identification: A linear matrix inequality approach," *Int. J. Robot. Res.*, vol. 33, no. 6, pp. 931–944, May 2014.

SHOUJUN WANG received the M.Tech. degree in hydraulics and pneumatics from Zhejiang University, in 1989. He is currently a Professor and the Dean of the Mechanical Engineering College, Tianjin University of Technology. He has published over 100 articles. He led more than 60 research projects, sponsored by the Ministry of Transport, the Ministry of Science and Technology, and universities and research institutes, to develop intelligent robots and marine power environment generation technologies. His research interests include the research and development of fluid transmission and control, electromechanical system integration, and unit technology. He is a Senior Member of the Chinese Mechanical Engineering Society and the Executive Director of the China Marine Engineering Society.

XINGMAO SHAO was born in Weifang, Shandong, China, in 1996. He received the B.Tech. degree in mechanical engineering from Liaocheng University, China, in 2018. He is currently pursuing the M.Tech. degree with the Tianjin University of Technology, China. His current research interests include inverse dynamic and intelligent algorithm of robot.

LIUSONG YANG received the M.Tech. degree from the Henan University of Science and Technology, in 2007. He is currently the Director of the Simulation Analysis and Industrial Design Center, CITIC Heavy Industries Company, Ltd. He presided over or participated in two provincial-level scientific research projects, obtained more than ten authorized invention patents, and published nearly 20 articles.

NAN LIU was born in Tianjin, China, in 1986. He received the B.Tech. and M.Tech. degrees in mechatronic engineering from the Tianjin University of Technology, in 2009 and 2012, respectively. He is currently pursuing the Ph.D. degree with Tianjin Polytechnic University. He has been a Lecturer with the Tianjin University of Technology, since 2012. He has published around ten research papers in international journals and conferences. His research interests include robotic dynamics and intelligent control for smart cities and factories. In addition, his research interests include wave theory and technology.